RHESSI Observations of Particle Acceleration and Energy Release in an Intense Solar Gamma-Ray Line Flare

R. P. Lin[1,2], S. Krucker[1], G. J. Hurford[1], D. M. Smith[1], and H. S. Hudson[1], G. D. Holman[3], R. A. Schwartz[3], B. R. Dennis[3], G. H. Share[4] and R. J. Murphy[4], A. G. Emslie[5], C. Johns-Krull[6], N. Vilmer[7]

,

ABSTRACT

We summarize RHESSI (Reuven Ramaty High Energy Solar Spectroscopic Imager) hard X-ray (HXR) and γ-ray imaging and spectroscopy observations of the intense (X4.8) γ-ray line flare of 23 July 2002. In the inital rise, a new type of coronal HXR source dominates that has a steep double power-law X-ray spectrum and no evidence for thermal emission above 10 keV, indicating substantial electron acceleration to tens of keV early in the flare. In the subsequent impulsive phase, three footpoint sources with much flatter double power-law HXR spectra appear, together with a coronal superhot (T $\sim$ 40 MK) thermal source. The north footpoint and the coronal source both move systematically to the north-northeast at speeds up to $\sim$50 km/s. This footpoint's HXR flux varies approximately with its speed, consistent with magnetic reconnection models, provided the rate of electron acceleration varies with the reconnection rate. The other footpoints show similar temporal variations, but do not move systematically, contrary to simple reconnection models.

---

[1]Space Sciences Laboratory, University of California, Berkeley, CA 94720 (rlin@ssl.ssl.berkeley.edu, krucker@ssl.berkeley.edu, ghurford@ssl.berkeley.edu, dsmith@ssl.berkeley.edu, hhudson@ssl.berkeley.edu)

[2]Also Physics Dept.

[3]NASA Space Goddard Flight Center, Greenbelt, MD 20771 (holman@stars.gsfc.nasa.gov, richard.schwartz@gsfc.nasa.gov, Brian.R.Dennis.1@gsfc.nasa.gov)

[4]Naval Research Laboratory (share@osse.nrl.navy.mil, murphy@osse.nrl.navy.mil)

[5]Dept. of Physics, The University of Alabama in Huntsville, Huntsville, AL 35899 (emslieg@email.uah.edu)

[6]Rice University, Houston, TX 77005 (cmj@rice.edu)

[7]Observatoire de Paris, Meudon, France (nicole.vilmer@obspm.fr)

γ-ray line and continuum emissions show that ions and electrons are accelerated to tens of MeV during the impulsive phase. The prompt de-excitation γ-ray lines of Fe, Mg, Si, Ne, C, and O - resolved here for the first time - show mass-dependent red shifts of $0.1-0.8\%$, implying downward motion of accelerated protons and alphas along magnetic field lines that are tilted toward the Earth by $\sim 40°$. For the first time, the positron annihilation line is resolved and the detailed high-resolution measurements are obtained for the neutron-capture line. The first ever solar γ-ray line and continuum imaging shows that the source locations for the relativistic electron bremsstrahlung overlap the 50-100 keV HXR sources, implying electrons of all energies are accelerated in the same region. The centroid of the ion-produced 2.223 MeV neutron capture line emission, however, is located $\sim 20 \pm 6$ arcseconds away, implying that the acceleration and/or propagation of the ions must differ from that of the electrons.

Assuming that Coulomb collisions dominate the energetic electron and ion energy losses (thick-target), we estimate a minimum of $\sim 2 \times 10^{31}$ ergs is released in accelerated $\sim$20 keV electrons during the rise phase, with $\sim 10^{31}$ ergs in ions above 2.5 MeV and about the same in electrons above 30 keV released in the impulsive phase. Much more energy could be in accelerated particles if their spectra extend to lower energies.

Subject headings:

1. Introduction

The Sun is the most energetic particle accelerator in the solar system, producing ions up to tens of GeV and electrons to tens of MeV. Large solar flares are the most powerful explosions in the solar system, releasing up to $\sim 10^{32}-10^{33}$ ergs in $\sim 10^{2}-10^{3}$ s. The accelerated 10-100 keV electrons (Lin and Hudson 1976) and sometimes $>\sim$1 MeV/nucleon ions (Ramaty et al. 1995) appear to contain a significant fraction, $\sim$10-50%, of this energy, indicating that the particle acceleration and energy release processes are intimately linked. Flare-accelerated electrons and ions colliding with the ambient solar atmosphere produce bremsstrahlung HXR/γ-ray continuum and γ-ray line emission, respectively. The NASA Reuven Ramaty High Energy Solar Spectroscopic Imager (RHESSI) Small Explorer (SMEX) mission (Lin et al. 2002) is designed to provide high resolution imaging (as fine as $\sim$2 arcsec) and spectroscopy ($\sim$1 keV FWHM) from soft thermal X-rays ($\sim$3 keV) to gamma-rays (17 MeV). In this issue of Astrophysical Journal Letters, RHESSI observations of the intense solar flare of 23 July 2002 are presented, including the first detailed hard X-ray imaging spectroscopy, the first high-resolution spectroscopy of solar γ-ray lines, the first imaging above 100 keV, and the first imaging of solar γ-ray lines.

2. Experimental Details

At HXR and γ-ray energies, unlike soft X-rays, EUV, and longer wavelength emissions, focusing optics are not presently feasible. The only viable method of obtaining arcsecond-class images in HXRs and γ-rays within the SMEX constraints is with Fourier-transform imaging (Makashima et al. 1977; Kosugi et al. 1991). The RHESSI imager (Hurford et al. 2002) is made up of nine bi-grid rotating modulation collimators (RMCs), each consisting of a pair of widely separated grids mounted on a rotating spacecraft, to provide spatial resolution of 2.3 arcsec to 3 arcmin over the full Sun ($\sim$1 deg.) field of view. Behind each RMC is a coaxial germanium detector (GeD). As the spacecraft rotates ($\sim$15 rpm), the RMCs convert the spatial information from the source into temporal modulation of the photon counting rates of the GeDs.

The GeDs (Smith et al. 2002) are cooled to $<\sim$75 K to achieve spectral resolution of $\sim$1 keV FWHM in the hard X-ray range, increasing to $\sim$4 keV FWHM at $\sim$2 MeV, the best ever achieved for solar measurements. The GeDs are segmented into a thin ($\sim$1.5 cm thick) front segment that stops photons from soft X-rays (3 keV) up to $\sim$300 keV, and a thick rear segment ($\sim$7 cm) for $>$300 keV to 17 MeV photons. This allows the γ-ray spectrum to be measured with low dead time, even in the presence of the intense X-ray fluxes. In addition, when the count rates exceed preset thresholds, a thin ($\sim$10 keV cutoff) shutter (in throughout this flare) and a thick one ($\sim$15 keV cutoff) are inserted automatically in front of the GeDs to attenuate low energy fluxes. The electronics is designed to eliminate pulse pile-up, but in very intense flares such as 23 July 2002, that have steep spectra and count rates exceeding 10^4 c/s per detector, spectral distortions can still be significant.

The energy and time (to a μs) of, every photon interaction, together with pointing information to $<\sim$arcsec, are stored in a 4 Gigabyte solid-state memory, sized for the largest flare. RHESSI was launched on February 5, 2002, into a nearly circular, 38° inclination, 600-km altitude orbit, and flare observations began a week later.

3. Overview of Flare

The intense (GOES class X4.8, optical importance 2B) 23 July 2002 solar flare began at $\sim$0018 UT in NOAA active region AR#0039 at S13E72 (NOAA Solar Geophysical Data).

The Hα, microwave radio, and HXR emissions all peaked at $\sim$0028-31 UT, with GOES soft X-rays peaking later, at 0035UT. Starting at $\sim$0025 UT, type III radio bursts were detected by ground observatories and by the Wind spacecraft, followed by type II and IV emission. An associated fast (2180km/s) and wide Coronal Mass Ejection (CME) was observed by the LASCO coronagraph on the SOHO spacecraft, but no solar energetic particle (SEP) event was detected in the interplanetary medium. For at least an hour before the flare, the Nobeyama Radioheliograph (NoRH) observed a large elongated loop structure extending $\sim 80''$ to the northeast, at both 17 and 34 GHz (White et al. 2003). This emission is consistent with an optically thin thermal source, but it is not observed by TRACE at 195Å, suggesting it is hotter than $\sim$1.5 MK. At the base of this loop, a bright compact source is detected at 17GHz but not at 34GHz, implying non-thermal emission.

The RHESSI observations of the flare HXR and γ-ray emission (Figure 1) divide naturally into a rise phase ($\sim$0018 to $\sim$0027UT) dominated by a coronal HXR source that appears to be non-thermal, an impulsive phase ($\sim$0027 to $\sim$0043 UT) with continuum and γ-ray line emission extending up to $>\sim$7 MeV, and a decay phase ($>\sim$0043UT) dominated by a superhot ($\sim$40 MK) thermal source (but with a HXR burst at $\sim$0050 UT). RHESSI's very high spectral resolution ($\sim$1 keV FWHM) and energy coverage down to thermal plasma (3 keV threshold) allow detailed measurements of the thermal/non-thermal transition. For this flare, the spatially-integrated HXR spectra up to $\sim$300 kev, determined every 20 s, have been forward-fit with a model consisting of an isothermal plasma component plus a double power-law non-thermal electron component at high energies (Holman et al. 2003). The spatial distribution of HXR sources (Krucker et al. 2003) is shown superimposed on TRACE 195A images, together with the simultaneous spatially integrated X-ray spectra, in a movie at: http://hesperia.gsfc.nasa.gov/hessi/presentations/video/

4. Rise Phase

The earliest rise above background in the RHESSI 12-20 keV and GOES 0.5-4 A channels is at $\sim$0018 UT. The HXR emission above 10 keV is concentrated in a coronal source about $22''$ in diameter located at (880-890$''$ E, 240-250$''$ S) (Figure 2a), about where the pre-flare compact 17 GHz radio source was located. This source generally has no chromospheric counterpart observed in TRACE 195Å, SOHO MDI white light or Hα images (Krucker et al. 2003). Brightenings in 195Å emission (also in Hα) are detected along three approximately N-S aligned flare ribbons, located $\sim 40''$, $\sim 10''$, and $\sim 20''$ west of the coronal hard X-ray source, beginning at $\sim$0021, 0023, 0024 UT, respectively. Some $>$10 keV HXR emission is detected sporadically from these ribbons, but it is always weaker than the coronal source.

The HXR spectra (Figure 2b) fit to a double-power-law shape, with exponents of typically $\gamma_L \sim 5$ below and $\gamma_H \sim 6.5$ above a relatively sharp break at energies varying from $E_b \sim 20$ to ~ 35 keV. This clearly does not fit to an isothermal spectrum, although, in principle, a distribution of thermal sources with a range of temperatures might be able to reproduce the double power-law spectral shape. Such a break can be produced if the electrons stop in a non-uniformly ionized target (Brown et al. 2003; Kontar et al. 2002). Since this source is mostly confined to the ionized corona, the observed break must be intrinsic to the accelerated electron spectrum.

In the rise phase before 0026:08 UT, there is no spectral evidence for a thermal component above 10 keV. Assuming thick-target emission in a cold ambient medium ($E_e \gg kT$), the energy deposited by the electrons above $\sim$10 keV, integrating over time from the rise to $\sim$0026UT, is estimated (Lin and Hudson 1976) to be $> \sim 4 \times 10^{32}$ ergs. By making the ad hoc assumption that a hot thermal plasma is present and choosing the highest low energy cutoff ($\sim$20 keV) that still fits the data, Holman et al. (2003) obtain a lower limit to the energy released in nonthermal electrons of $\sim 2 \times 10^{31}$ ergs. Since only a small fraction of the HXR emission is observed from footpoints along the TRACE ribbons, most of the energetic electron energy appears to be deposited into the coronal source.

The GOES soft X-ray time profile during the rise phase is similar to the time integral of the RHESSI HXR (12-25 keV) flux [i.e., the "Neupert" effect (Neupert 1968)] - consistent with the energetic electrons colliding with the dense solar chromosphere in the footpoints, heating and evaporating the gas to form the high temperature plasma. The GOES measurements at 0026 UT fit to a temperature of $\sim$19 MK and an emission measure of 1.6×10^{49} cm^{-3}. Assuming that the GOES source is co-spatial with the RHESSI HXR source [soft X-ray imaging is not available], whose volume is V = $\sim 4 \times 10^{27}$ cm^3, corresponding to $\sim (22'')^3$, we obtain a thermal plasma density of $\sim 6 \times 10^{10}$ cm^{-3} and an energy content in the soft X-ray plasma of only $\sim 10^{30}$ ergs, much less than the integral of the non-thermal electron energy over time. Even assuming that the GOES thermal source volume is ten times larger only increases the thermal energy to $\sim 3 \times 10^{30}$ ergs.

For an ambient density of $\sim 6 \times 10^{10}$ cm^{-3}, the density of non-thermal electrons is $\sim 6 \times 10^7 cm^{-3}$ (Holman et al. 2003) and the e-folding energy loss time for 20-100 keV electrons is $\sim$0.05-0.5 s (Lin 1974), implying that the primary flare energy release during the rise phase is going into accelerating electrons to continuously replenish the coronal source.

5. Impulsive Phase

At ~0026:15 UT there is an abrupt increase in the HXR emission and a change in its character; the thick shutter is inserted at this time. A "superhot" (~40 MK) thermal spectrum begins to dominate below ~30 keV (Figure 2d). At the same time the centroid of the 12-30 keV source shifts to the northeast by ~6 arcsec, suggesting that this superhot source is not co-spatial with the rise-phase coronal non-thermal source (Figure 2c). By ~0027:30 UT when the centroid of the coronal source is at 887″E, 235″S, strong emission is observed in three footpoints - north (initial centroid 866″E, 230″S from Sun center), south (869″E, 243″S), and middle (873″E, 233″S) - each with a chromospheric counterpart observed in Hα, EUV (TRACE), and white light (SOHO MDI) (Krucker et al. 2003). The spatially integrated X-ray spectra (Figure 2d), although still double power-law above ~30 keV, are much harder (HXR γ_L and γ_H $\sim 2.5 - 3.5$) than those of the rise phase coronal source, with typical break energies from ~70 to >100 keV (Holman et al. 2003).

The north and south footpoints are located in opposite polarity magnetic field from SOHO MDI magnetograph), separated by ~13″ (~10,000 km). Krucker et al. (2003) found that the temporal variations of the X-ray fluxes of these two footpoints track each other closely in time, to within seconds over the impulsive phase (to 00:40 UT), suggesting that they are at opposite ends of the same magnetic loops. During the first (and most intense) burst, the north footpoint rapidly moves north-northeast, roughly parallel to the magnetic neutral line, at speeds up to ~50 km/s. The motions are only apparent; the HXR emission is shifting to the adjacent footpoints of newly reconnected field lines. The intensity of the north footpoint's HXR emission is observed generally to vary with its speed (Krucker et al. 2003). These observations indicate that magnetic reconnection is occurring in the corona, forming new magnetic loops that join the north and south footpoints. The rate of reconnection should vary as the speed of the footpoint if the magnetic field strength is roughly constant. The rate of electron acceleration appears to vary with the rate of reconnection.

The superhot coronal source also moves in the same direction with a comparable speed (Krucker et al. 2003). Initially, the superhot source appears to exhibit the Neupert effect. After ~0029UT, however, its intensity stays nearly constant, through the next burst at 0031UT. The coronal source location - ~20″ east of the north and south footpoints, which themselves are only separated by ~13″ - suggests that it may be above the loop connecting these two footpoints, in the cusp formed by just reconnected field lines. Thus, the superhot source may be due to heating by the reconnection jets.

Although these general features support the reconnection picture, there are many puzzling details which indicate a much more complicated picture (see also Fletcher and Hudson (2002)). The south footpoint and the middle footpoint (same polarity as the south footpoint) stay nearly stationary with occasional abrupt jumps. The HXR flux of the middle footpoint only varies with the north footpoint until 00:30:30 UT, and its HXR emission disappears after ∼00:32:30 UT. Furthermore, in both the first impulsive burst (∼0027:30- 0030 UT) and the second (0034:30-0037 UT), the north footpoint's HXR flux peaks before the speed reaches its maximum (Krucker et al. 2003).

HXR spectra obtained separatedly for the north, south, and middle footpoint sources (Emslie et al. 2003), were fit to single X-ray power-laws above ∼50 keV (to avoid pulse-pileup effects not yet corrected for the individual sources). The power-law exponents of the north and south footpoints were found to show the same temporal variations through most of the impulsive phase, but with the north footpoint's exponent being systematically ∼0.3-0.4 larger. This difference could be the result of the acceleration mechanism, or it may indicate that the column density from the common accelerated electron source to the south footpoint is greater by a factor of $\sim 1.5 - 2$ than to the north source, so that Coulomb collisions will harden the electron spectrum by a greater amount in the south than in the north. The difference in column density could be due to the location of the acceleration region farther from the south source, a greater density in the leg of the loop toward the south source, or a larger pitch angle for the electrons streaming toward the south source. The middle source begins with the same spectral exponent as the north source, but then becomes $\sim 0.3 - 0.4$ greater. If it is also linked magnetically to the north source, the difference in spectral index might be accounted for in a similar way.

6. γ-ray Line Emission

Flare-accelerated protons and alpha particles colliding with ambient carbon and heavier nuclei produce narrow prompt de-excitation lines (widths of ∼few keV to ∼100 keV), while accelerated heavy nuclei colliding with ambient hydrogen and helium produce much broader lines that merge together to form a nuclear "continuum" (Ramaty and Murphy 1987). The collisions also produce neutrons, positrons, and pions. Neutron capture on hydrogen and positron annihilation yield narrow lines at 2.223 MeV and 0.511 MeV, respectively, both of which are delayed.

γ-ray line emission has been detected from many large solar flares (Chupp 1990; Share and Murphy 1995; Share et al. 2002). In this flare, the γ-ray line emission occurred predominantly during the impulsive phase (0027-0040 UT). Figure 3 shows the background subtracted $\sim 0.3 - 10$ MeV γ-ray count spectrum, integrated over this time interval, with a preliminary fit to the various components - bremsstrahlung continuum, narrow and broad prompt de-excitation γ lines, the delayed neutron capture and positron annihilation lines, and the alpha-alpha lines - taking into account the full instrument response matrix including the off-diagonal elements.

The narrow prompt de-excitation lines of Fe, Mg, Si, Ne, C, and O are resolved for the first time (Smith et al. 2003). The line centroids exhibited significant Doppler red-shifts from $\sim$0.1 to 0.8%, and line widths of 0.1-2.1% (FWHM) were measured. Both these quantities generally decrease with mass of the emitting nucleus, as expected since heavier nuclei will recoil less from a collision with a fast proton or alpha particle. The red shifts, however, are too large for ions traveling downward in a radial magnetic field at the optical flare location. Assuming a model of accelerated ions with an isotropic distribution in the downward hemisphere along the magnetic field, the best fit gives a field direction tilted by $\sim 40^\circ$ from radial, toward the observer. For a narrow beam, the field could be nearly radial, but RHESSI's measurement of the γ-ray line complex from accelerated alphas fusing with ambient helium (Share et al. 2003a) is inconsistent with a narrow beam.

Fast neutrons from energetic ion collisions thermalize in the photosphere before being captured by hydrogen to form deuterium, which then emits a 2.223 MeV photon. RHESSI has made the first detailed high resolution measurement (with the instrumental resolution at $\sim$2 MeV of $\sim$4 keV FWHM) of this very narrow (intrinsic width $<\sim$0.1 keV) line (Murphy et al. 2003, Figure 3). The line flux, measured every 20s, was fit to a physically-based model (Hua et al. 2002) of an accelerated ion source (whose temporal profile is given by the prompt lines) in a magnetic loop with field perpendicular to the surface at the footpoints, and taking into account pitch-angle scattering of the ions in the corona. Such a model can be used to constrain the solar ^{3}He abundance, since ^{3}He will also capture neutrons but without emitting a 2.223 MeV photon. Although reasonably good agreement can be obtained for some parameters, an improved model is needed since we know from the red shifts in the prompt lines that the field is inclined from normal to the surface. Preliminary analysis indicates that energetic neutrons may have been detected from this flare (B. Barraclough, private commun., 2003).

RHESSI has obtained the first direct information on the location and spatial extent of the energetic ion interaction region in a solar flare (Hurford et al. 2003). The two rotating modulation collimators (RMCs) with 2 and 3 cm thick tungsten grids ($35''$ & $180''$ resolution respectively) were used to obtain images in four energy bands for the same time interval and using the same imaging parameters: 2.218 – 2.228 MeV for the 2.223 MeV line, 3.25 – 6.5 MeV to include the prompt de-excitation lines of C and O, and 0.3 – 0.5 and 0.7 – 1.4 MeV dominated by electron-bremsstrahlung. The imaging at $180''$ resolution showed that the sources in all the bands were near the optical flare.

Using both thick RMC's, the 2.223 MeV line source was determined to be less than $\sim$1 arcmin size, and its centroid was found to be displaced by ∼20 (±6) arcsec (∼14,000 km) from the centroid of the $0.3-0.5$ MeV (and $0.7-1.4$ MeV) electron bremsstrahlung sources (Figure 4). Models indicate that the 2.223 MeV line source should be within ∼500 km (<1 arcsec) of the energetic ion interaction region (Hua et al. 2002), and thus it is a good tracer of the energetic ions. The separation of the centroids clearly implies a difference in acceleration and/or propagation between the accelerated electron and ion populations near the Sun. No significant HXR emission was detected near the 2.223 MeV centroid, which is south and limbward of all the HXR sources. No significant flare Hα emission was observed at the centroid, although weak Hα emission is seen both to the east and west.

Flare-accelerated ions interact with the solar atmosphere to produce radioactive nuclei (and pions) that decay with the release of a positron. The positrons then slow down through Coulomb collisions and annihilate in flight, emitting two photons at 511 keV, or they capture an electron to form positronium in either the singlet or triplet state. Annihilation from the singlet state also produces two 511 keV photons but annihilation from the triplet state produces three photons with a continuum of energies up to 511 keV. The line shape and the $3\gamma/2\gamma$ ratio depend on the temperature, density, and composition of the medium where these processes take place. RHESSI has made the first high-resolution measurement of the positron annihilation line (Share et al. 2003b). The observed approximately Gaussian shape and measured width of 8.1±1.1 keV FWHM are consistent with positronium formation by charge exchange in flight with neutral hydrogen at ∼6000±300 K, or with free annihilation in a hot $\sim 4-7\times10^5$ K plasma. The observed upper limit to the $3\gamma/2\gamma$ ratio is only marginally consistent with the former, and the latter requires an implausibly large atmospheric column density at transition region temperatures.

7. Discussion

This flare shows two clearly different acceleration and energy releases: 1) a coronal acceleration of electrons to tens of keV in the rise phase, identified here for the first time although possibly observed before (Alexander and Metcalf 1997) but not recognized as non-thermal since high spectral resolution was not available; and 2) the more common impulsive phase acceleration that apparently is related to magnetic reconnection. Although there is a coronal source present at this time, perhaps above the loop-top, it is a superhot thermal source, unlike the non-thermal source of Masuda et al. (1994).

In the rise phase, substantial numbers of electrons are accelerated in the corona with a steep double power-law (electron spectrum $\delta_L =\sim 6$, $\delta_H =\sim 8$) with break energies of $\sim 50-60$ keV. Only a small fraction of these electrons reach the chromosphere; presumably most of them deposit their energy into the corona. No γ-ray line emission is detected, so there is no significant ion acceleration to tens of MeV energies.

During the impulsive phase, the accelerated electron spectrum becomes much harder, with electron power law exponents $\delta_L = \sim$2.5-3.5, $\delta_H = \sim$4-4.5, and break energies of $\sim$110-150 keV. Above $\sim$500 keV there appears to be another electron component extending to >7 MeV, with a flatter spectrum. Detailed ($\sim 7''$) imaging of the $0.3 - 0.5$ MeV band (Fig. 4 black contours) shows that these emissions overlap the $50 - 100$ keV hard X-ray sources, but are more concentrated toward the limb where the south footpoint, which has the flatter spectrum, is located. Thus, the electrons from tens of keV up to relativistic energies appear to be accelerated in the same regions. Preliminary timing analyses indicate that the MeV bremsstrahlung continuum may lag the hard X-ray continuum by $\sim$10s.

The rate of energy deposition by the accelerated electrons peaks at $\sim 10^{29}$ ergs/s above $\sim$20 keV during the rise phase and drops to $\sim 2\times10^{28}$ ergs/s at the start of the impulsive phase, decreasing to below 10^{28} ergs/s by 0040UT (Holman et al. 2003). It should be emphasized that these are lower limits to the energy in electrons. If the low energy cutoff is 10 keV during the rise phase, the total energy (and power) in accelerated electrons would go up by about an order of magnitude.

Emslie (2003) shows that, in principle, a low energy cutoff, is not necessary for a warm plasma. Electrons with energies below $\sim$5 kT lose significantly less energy than in the cold target approximation, with the energy loss rate dropping to zero at $\sim$kT. Using his formulas we obtain $\sim 4\times10^{34}$ ergs as the upper limit to the total energy released in all accelerated electrons for kT$\sim$2 keV. This is far more energy than ever deduced even for the largest flares, but a larger kT would reduce this estimate significantly.

Information on the spectrum of the accelerated ions can be obtained from comparing γ-ray line fluences. This flare emitted 28.6$\pm$13, 21.4$\pm$4.5, 192.6$\pm$4.8 and 163$\pm$14 photons/cm^2 in the C line, the Ne line, the neutron capture ^{2}H (2.223 MeV) line, and the $4-7$ MeV band, respectively. Assuming that the accelerated ion spectrum is a single power-law extending down to 2.5 MeV/nucleon, the ^{2}H/4-7, ^{2}H/Ne, and ^{2}H/C fluence ratios give power-law exponents of 3.4$\pm$0.1, 3.8$\pm$0.1, and 4.0$\pm$0.5, respectively. Taking the middle value, we obtain a minimum total energy in accelerated protons above $\sim$2.5 MeV (the threshold for the Ne line) of $\sim 1.4\times10^{30}$ ergs, and in all accelerated ions (protons plus heavier nuclei) of $\sim 10^{31}$ ergs. Here we have assumed the cross-sections and energy loss modeling of Murphy et al. (1988), and "impulsive flare" abundances (Ramaty et al. 1996) with alpha/proton = 0.5, alpha/O = 50 and ^{3}He/^{4}He = 1; this will be checked with more detailed future analysis.

Assuming a thick target, we obtain a rate of energy deposition by energetic, $>\sim$2.5

MeV/nucleon ions of $\sim 1.5\times10^{28}$ ergs/s in the first 4 minutes of the impulsive phase, dropping to $\sim 5\times10^{27}$ ergs/s in the following 10 minutes. Thus, a comparable amount of energy is being deposited by accelerated >2.5 MeV/nucleon ions as by accelerated >30 keV electrons during the impulsive phase.

The time history of the $3.25-6.5$ MeV nuclear prompt line emission is generally similar (with a lag of ∼10s) to the $0.3-0.5$ and $0.7-1.4$ MeV electron bremsstrahlung bands (Fig. 1 in Hurford et al. 2003). This similarity has been seen before in other γ-ray flares, e.g. 7 June 1980 (Chupp 1990), and it suggests a common acceleration for electrons and ions. If they are accelerated and transported similarly, however, the ion-associated gamma-ray source would be expected to coincide spatially with the electron-bremsstrahlung source. The centroid of the 2.223 MeV line appears to be in a positive polarity magnetic region, at one foot of large-scale post-flare loops (Figure 4). The three hard X-ray footpoints and the coronal source seen in the impulsive phase is inside these large-scale loops, likely on an inner arcade of loops. One way of separating ion from electrons is by a large-scale quasi-static electric field. Another possibility, consistent with the observed delay of ∼10s of the ions relative to the electrons, is that the acceleration of the electrons and/or their subsequent interactions with the ambient medium produced a disturbance which propagated into these higher loops and accelerated the ions. Also, stochastic acceleration processes may favor shorter loops for electron acceleration (Miller, 2000).

Johns and Lin (1992) showed that precise high resolution measurements of optically thin hard X-ray spectra can be directly inverted to obtain the spectra of the parent X-ray producing electrons (assumed isotropic) averaged over density (also referred to as mean electron flux spectra, Brown et al. (2003) or thin-target spectra), without assumptions about physical conditions in the emission region. The precise measurements of the spatially-integrated spectra provided by RHESSI, especially for intense flares, allow the first application of these analysis techniques. Piana et al. (2003) have devised a regularized inversion algorithm that yields the smoothest electron flux spectrum consistent with the data, while retaining real features. These results show promise, but caution must be exercised since small (of order 1%) uncertainties in the X-ray spectrum (such as those due to albedo, non-uniform target ionization, corrections for pulse pile-up, etc.) can lead to large uncertainties in the inferred electron spectra.

Kontar et al. (2003) find that during the impulsive phase of this flare, the high resolution HXR spectra deviate from a power-law behavior in a manner consistent with non-uniform target ionization. Schmahl and Hurford (2002) have shown that RHESSI may be able to image albedo patches. RHESSI is also capable of measuring the polarization of the HXRs (∼20-200 keV) through scattering from a well-placed passive beryllium scattering cylinder into the rear segments of the surrounding GeDs (Smith et al. 2002; McConnell et al. 2003), and of gamma-rays ($\sim$0.15-2 MeV)through scattering directly from one GeD to another GeD (see Coburn and Boggs 2003). These measurements will provide information on the electron anisotropy. Such studies, together with other measurements (i.e. radio imaging and spectroscopy (White et al. 2003) and with optical (Firstova et al. 2003) polarization) will provide further constraints on the processes of energy release and particle acceleration in flares.

This research effort is supported in part by NASA contract NAS5-98033. RHESSI is named in honor of Dr. Reuven Ramaty - a Co-I and a pioneer in the fields of solar physics, gamma-ray astronomy, nuclear astrophysics, and cosmic rays - who passed away before the HESSI launch.

REFERENCES

Alexander, D., and Metcalf, T. R. 1997, Astrophys. J., 489, 442.

Brown et al. 2003, Astrophys. J. Lett., this volume.

Chupp 1990, Phys Scripta, T18, 15.

Coburn and Boggs 2003, Nature, 423, 415.

Emslie 2003, Astrophys. J. Lett., this volume.

Emslie et al., 2003, Astrophys. J. Lett., this volume.

Firstova et al. 2003, Astrophys. J. Lett., this volume.

Fletcher, L. and Hudson, H.S., 2002, Solar Physics, 210, 307.

Holman et al. 2003, Astrophys. J. Lett., this volume.

Hua et al. 2002, Astrophys. J. Suppl., 140, 563.

Hurford, G., et al. 2002, Solar Phys, 210, 61.

Hurford, G., et al. 2003, Astrophys. J. Lett., this volume.

Johns, C., and Lin, R. P. 1992, Solar Phys., 137, 121.

Kontar et al. 2002, Solar Phys, 210, 419.

Kontar et al. 2003, Astrophys. J. Lett., this volume.

Kosugi et al. 1991, Solar Phys., 136, 17.

Krucker, S., et al. 2003, Astrophys. J. Lett., this volume.

Lin, R. P. 1974, Space Sci. Rev., 16, 189.

Lin, R. P., and Hudson 1976, Solar Phys., 50, 153.

Lin, R. P., et al. 2002, Solar Phys, 210, 3.

Makashima et al. 1977, New Instrumentations for Space Astronomy, K. A. van der Hucht and G. Vaiana, New York: Pergamon Press.

McConnell et al. 2002, Solar Phys, 210, 125.

Masuda et al. 1994, Nature, 371, 495.

Miller, J. A. 2000, "Stochastic Particle Acceleration in Solar Flares", in High-Energy Solar Physics: Anticipating HESSI, eds. R. Ramaty & N. Mandzhavidze (San Francisco: ASP, Vol. 206), p. 145.

Neupert, W. M. 1968, Astrophys. J., 153, L59.

Murphy et al., Astrophys. J., 331, 1029.

Murphy et al. 2003, Astrophys. J. Lett., this volume.

Piana et al. 2003, Astrophys. J. Lett., this volume.

Ramaty and Murphy 1987, Space Sci. Rev., 45, 213.

Ramaty, R., et al. 1995, Astrophys. J. Lett., 455, 193.

Ramaty, R., et al. 1996, AIP Conf. Proc. 374, R. Ramaty, N. Mandzhavidze, and X.-M. Hua, New York: AIP, 172.

Schmahl and Hurford 2002, Solar Phys, 210, 273.

Share and Murphy 1995, Astrophys. J., 452, 933.

Share et al., 2002, Astrophys. J., 573, 464.

Share et al. 2003a, Astrophys. J. Lett., this volume.

Share et al. 2003b, Astrophys. J. Lett., this volume.

Smith, D. M., et al. 2002, Solar Phys, 210, 33.

Smith, D. M., et al. 2003, Astrophys. J. Lett., this volume.

White et al. 2003, Astrophys. J. Lett., this volume.

This preprint was prepared with the AAS LaTeX macros v5.0.

Fig. 1.— RHESSI hard X-ray and gamma-ray count rates (counts-s^{-1}-detector^{-1}) for the 23 July 2002 flare. The rates are scaled to fit: 20-40 keV $\times$ 0.3; 40-80 keV $\times$ 0.07; 80-150 keV $\times$ 0.02; 150-400 keV; 400-800 keV $\times$ 0.001; 800-2218 keV $\times$ 0.0005; 2218-2228 keV $\times$ 0.01; 2228-7000 keV $\times$ 2×10^{-5}. The thick shutter is inserted at $\sim$0026, 0041, 0044, 0050 UT and removed at $\sim$0040, 0043, 0049 UT. The slow variation through the interval is due to background from cosmic ray interactions with the atmosphere and spacecraft.

Fig. 2.— a) RHESSI 12-30 keV image (contour levels 15, 30, 45, 60, 75, 90%) during the rise phase (0021:42UT) superimposed on the TRACE 195 Å image. b) RHESSI X-ray spectrum for 0021:42UT, with fit to isothermal (dotted line) and double power-law (dashed line) and sum (solid line). c) RHESSI image (black contours 12-18 keV, levels 15, 30, 45, 60, 75, 90%; white contours 30-80 keV, levels 30, 60, 70, 90%) at 0028:15UT during the impulsive phase, superimposed on a Hα image from Big Bear Solar Observatory. d) RHESSI X-ray spectrum for 0028:15UT, with fits as in (b).

Fig. 3.— The RHESSI gamma-ray count spectrum from 0.3 to 10 MeV, integrated over the interval 0027:20 - 0043:20 UT. The lines show the different components of the model used to fit the spectrum.

Fig. 4.— The RHESSI centroid of the 2.223 MeV line emission (red circle, indicating 1 sigma uncertainty) that indicates the energetic ion interaction region, superimposed on a TRACE image taken $\sim$90 minutes after the flare, showing the post-flare loops. The yellow and pink circles are the centroids (1 sigma) of the $300-500$ and $700-1400$ keV bands, respectively, dominated by bremsstrahlung emission. The black and blue contours show the detailed images at $300-500$ keV and $50-100$ keV, respectively; the $50-100$ keV centroid is indicated by the cross.

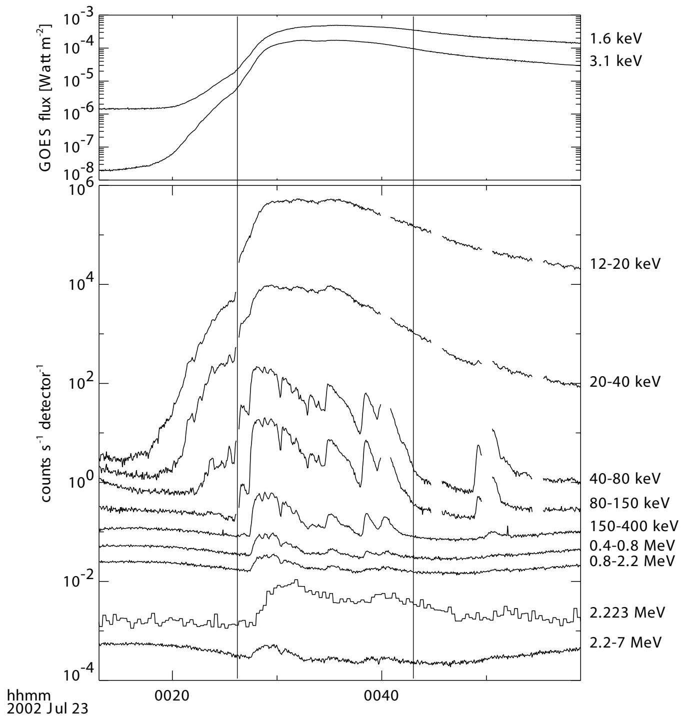

GOES flux [Watt m^-2]
1.6 keV
3.1 keV
counts s^-1 detector^-1
12-20 keV
20-40 keV
40-80 keV
80-150 keV
150-400 keV
0.4-0.8 MeV
0.8-2.2 MeV
2.223 MeV
2.2-7 MeV
hhmm
2002 Jul 23
0020
0040

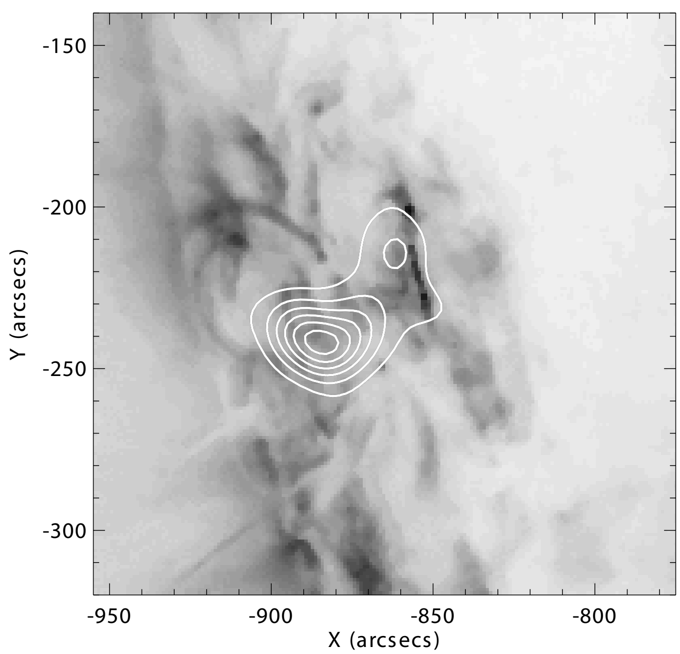

-150
-200
-250
-300
Y (arcsecs)
-950
-900
-850
-800
X (arcsecs)

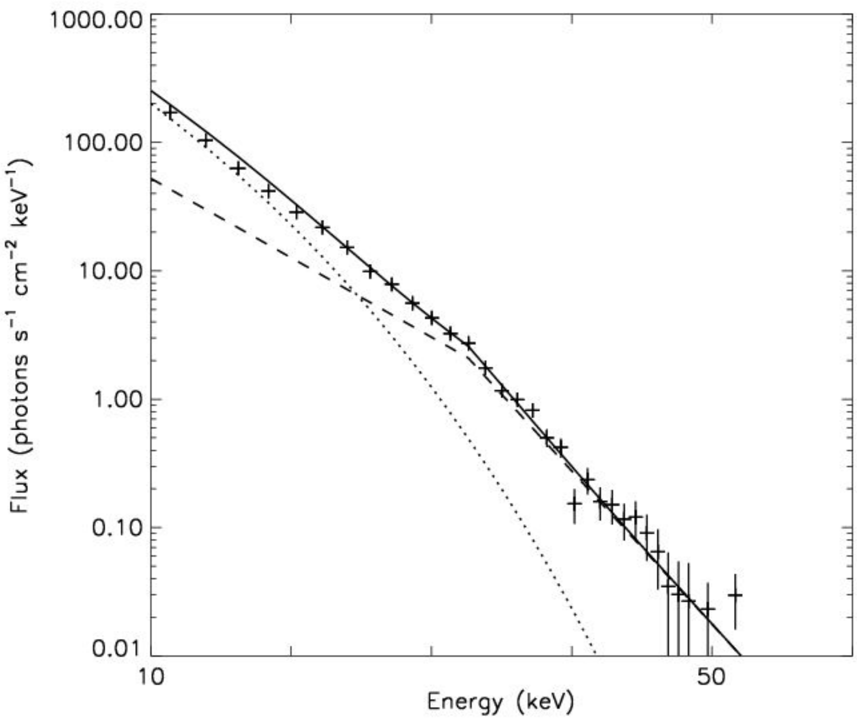

1000.00
100.00
10.00
1.00
0.10
0.01
Flux (photons s^{-1} cm^{-2} keV^{-1})
10
50
Energy (keV)

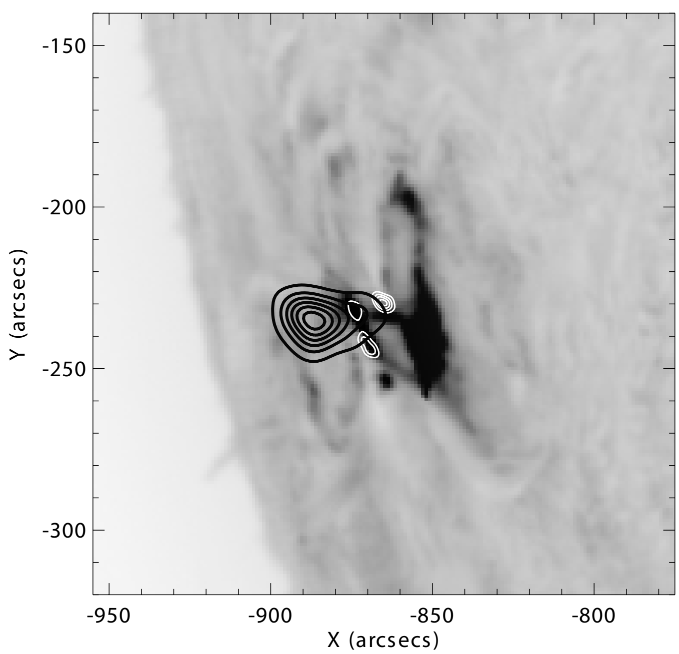

-150
-200
-250
-300
Y (arcsecs)
-950
-900
-850
-800
X (arcsecs)

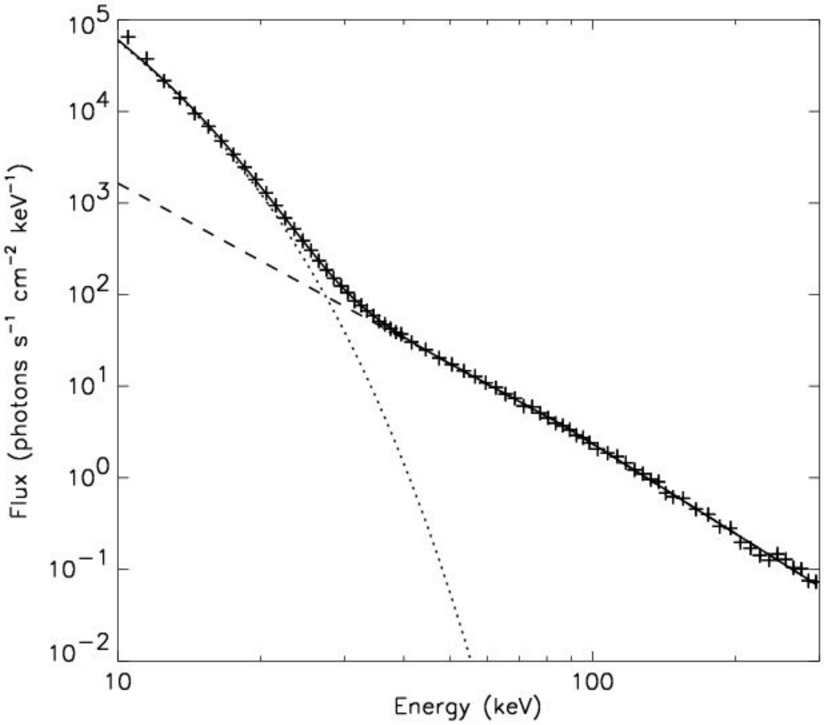

10^5
10^4
10^3
10^2
10^1
10^0
10^{-1}
10^{-2}
Flux (photons s^{-1} cm^{-2} keV^{-1})
10
100
Energy (keV)

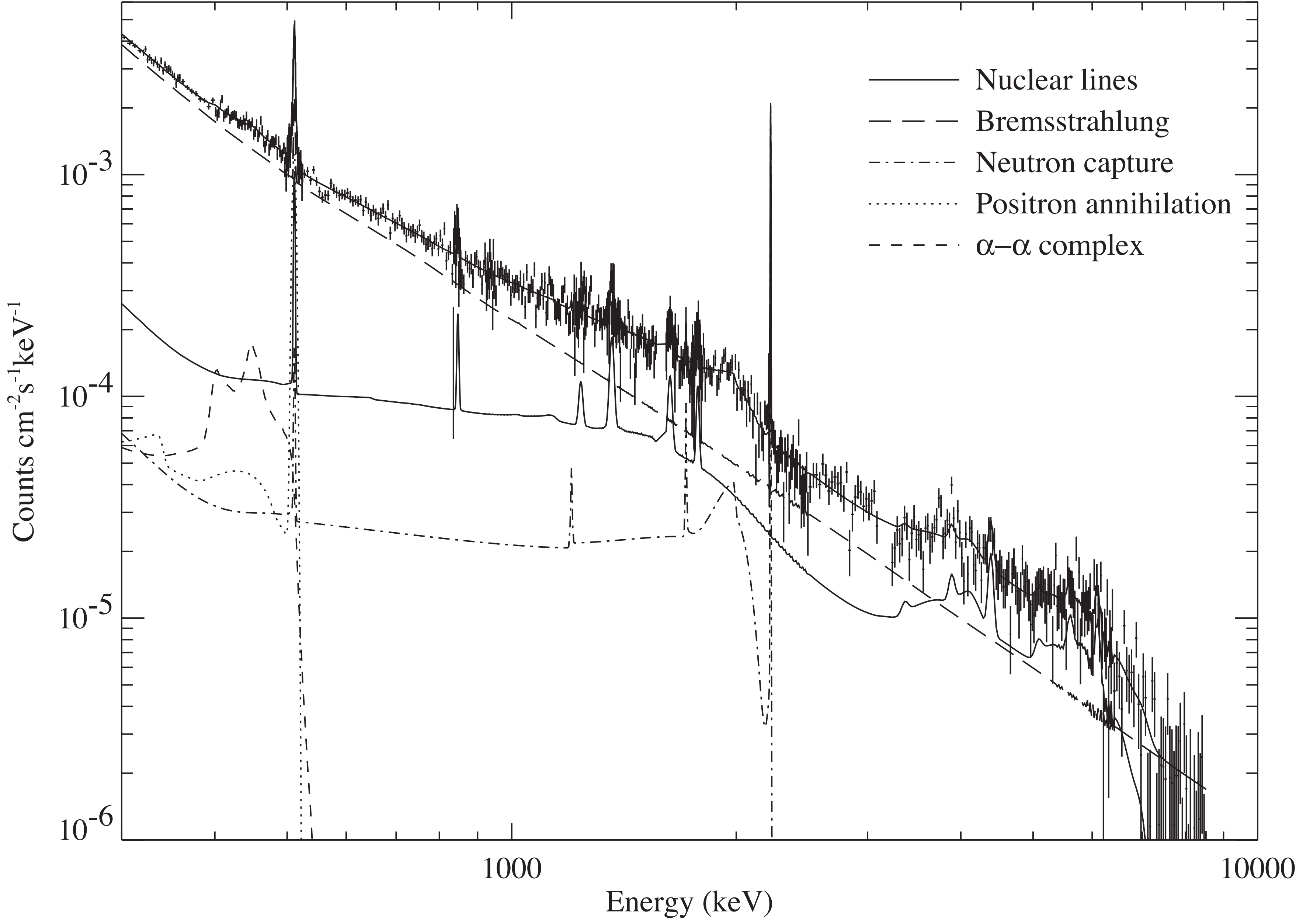

Nuclear lines
Bremsstrahlung
Neutron capture
Positron annihilation
α–α complex
Counts cm-2s-1keV-1
10-3
10-4
10-5
10-6
1000
10000
Energy (keV)

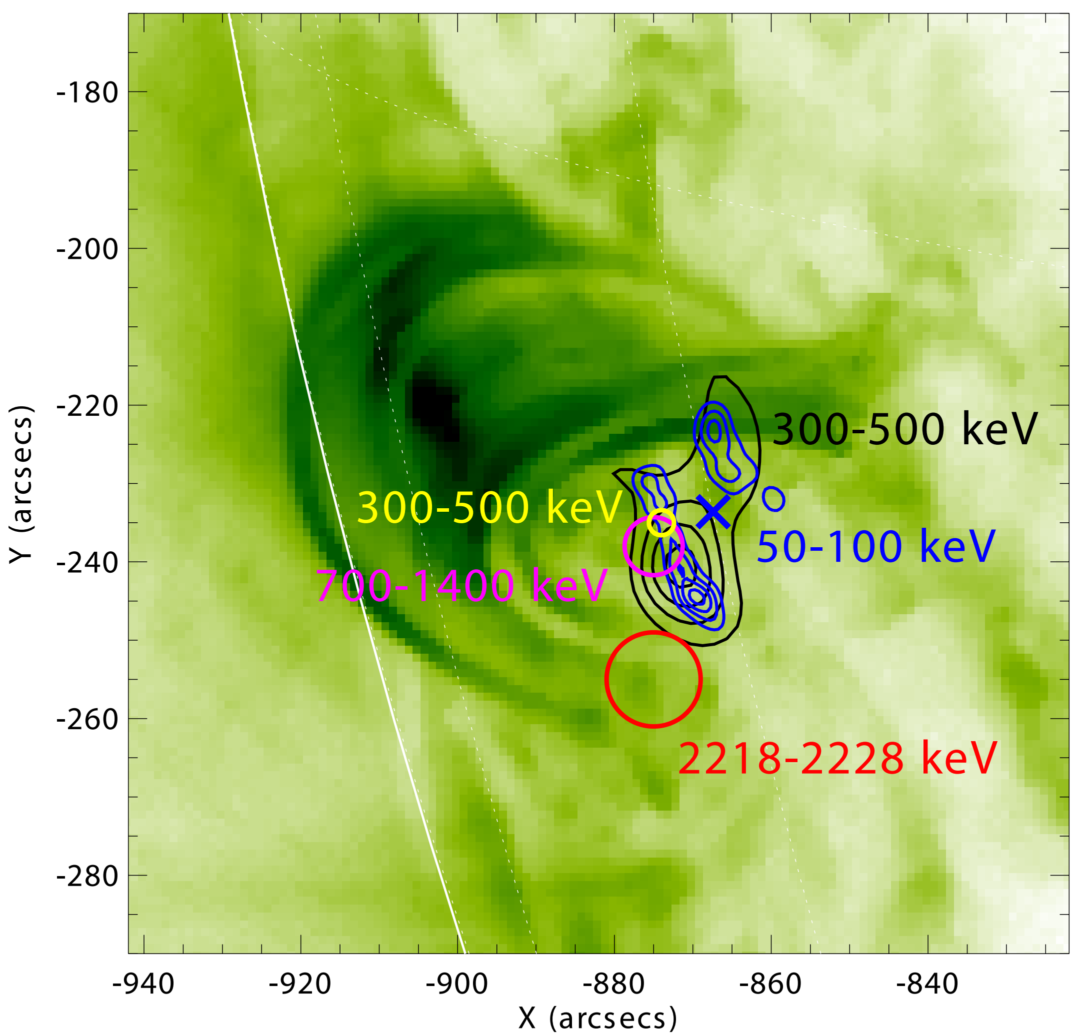

Y (arcsecs)
X (arcsecs)
-180
-200
-220
-240
-260
-280
-940
-920
-900
-880
-860
-840
300-500 keV
300-500 keV
50-100 keV
700-1400 keV
2218-2228 keV